Electronic Supplementary Material (ESI)

Graphite N-C-P dominated three-dimensional nitrogen and phosphorus co-doped holey graphene foams as high-efficiency electrocatalysts for Zn-air battery

Liping Ge,[a] Dan Wang,[a] Peixia Yang,*[a] Hao Xu,[a] Lihui Xiao,[a] Guo-Xu Zhang,*[a] Xiangyu Lu,[b] Zhenzhen Duan,[a] Fan Meng,[a] Jinqiu Zhang[a] and Maozhong An[a]

a MIIT Key Laboratory of Critical Materials Technology for New Energy Conversion and Storage, School of Chemistry and Chemical Engineering, Harbin Institute of Technology, 150001 Harbin, China.

b ZhuHai Coslight Battery Co., Ltd., 519180 Zhuhai, China.

* Corresponding authors: Peixia Yang (yangpeixia@hit.edu.cn); Guo-Xu Zhang (zhanggx@hit.edu.cn)

Experimental Section

Materials

Graphite flakes (95%) was purchased from Jixi Puchen Graphite Co. Ltd. Sulfuric acid (H_2SO_4), phosphoric acid (H_3PO_4), hydrogen peroxide (H_2O_2, 30%) and potassium permanganate ($KMnO_4$), melamine and urea were obtained from Sinopharm Chemical Reagent Co. Ltd. Phytic acid solution (50% in H_2O) and potassium hydroxide(KOH, 99.999%) was purchased from Shanghai Aladdin biochemical technology Co. Ltd. All chemicals were used without any further purification.

Synthesis of graphene oxide (GO)

Graphene oxide (GO) is synthesized by the improved Hummers method. A mixture of 200 mL of concentrated H_2SO_4 / H_3PO_4 ($V_{H_2SO_4}$: $V_{H_3PO_4}$ = 9: 1) was added to 1.5 g of graphite powder, followed by the addition of 9 g of $KMnO_4$ under vigorous stirring. After the reaction system was further heated at 50℃ for 6 hours, 20 mL of H_2O_2 (30%) was added. The above reaction system was then kept at 50℃ for 3 hours and then cooled to room temperature. The obtained suspension was washed by centrifugation several times, and then freeze-dried to obtain a graphite oxide sample. A certain amount of powdered graphite oxide is dissolved in ultrapure water, and ultrasonically dispersed to obtain a graphene oxide solution.

Oxygen Reduction Measurements.

After purging with pure N_2 or pure O_2 for at least 30 minutes, the catalyst ORR performance was investigated by LSV at a scan rate of 10 mV / s in a potential range of 0.2 V to 1.2 V (*vs*. RHE) and at 1600 rpm in a 0.1 M KOH solution. In addition, the

ORR polarization curves at different speeds (400, 900, 1600, 2500 rpm) were recorded. The number of transferred electrons (n) is calculated by the Koutechy-Levich (K-L) equation:

$$\frac{1}{j}=\frac{1}{j_{\mathrm{L}}}+\frac{1}{j_{\mathrm{K}}}=\frac{1}{B\omega^{\frac{1}{2}}}+\frac{1}{j_K} \tag{1}$$

$$B=0.2nFC_{\mathrm{O}}D_{\mathrm{O}}^{\frac{2}{3}}v^{-\frac{1}{6}} \tag{2}$$

Where j, j_{K} and j_{L} are measured current density, kinetic-limiting current and diffusion-limiting current density respectively; ω is the rotational speed (rpm) of RDE; F is the Faraday constant (96485 C mol^{-1}); C_{O} is the O_2 concentration (0.1M KOH is 1.2×10^{-3} mol L^{-1}); D_{O} is the diffusion coefficient of O_2 (0.1 M KOH is 1.9×10^{-5} cm^2 s^{-1}); v is the dynamic viscosity of 0.1 M KOH (0.01 cm^2 s^{-1})

In addition, a rotating ring disk electrode (RRDE) was used to determine the hydrogen peroxide yield (H_2O_2%) and electron transfer number (n), and the equation is as follows:

$$\mathrm{H_2O_2}(100\%)=200\frac{I_{\mathrm{R}}/N}{I_{\mathrm{D}}+I_{\mathrm{R}}/N} \tag{3}$$

$$n=4\frac{I_D}{I_{\mathrm{D}}+I_{\mathrm{R}}/N} \tag{4}$$

Where I_{D} is the disk current density, I_{R} is the ring current density, and N is the collection efficiency of the Pt ring (37%).

TOF calculation details

$$TOF(@0.85\mathrm{V\ versus\ RHE})(\mathrm{e\ site^{-1}\ s^{-1}})=\frac{i_K(@0.85\mathrm{V\ versus\ RHE})(\mathrm{A})}{n(\mathrm{mol})F(\mathrm{C\ mol^{-1}})}$$

Here, $i_K(@0.85\mathrm{V\ versus\ RHE})$ is kinetic-limiting current@0.85V versus RHE (A), F is

the Faraday constant (96485 C mol^{-1}), *n* is the number of active sites in catalysts (mol).

For example, for graphite N-C-P species,

$$(\text{graphite N - C - P})\ \text{at\%} = \text{P - C at\%} \times \frac{\text{graphitic N at\%}}{\text{Total N at\%}} = 0.2689\% \times \frac{0.9586\%}{2.83\%} = 0.0911\%$$

$$TOF(@0.85\text{V versus RHE})_{\text{graphite N - C - P}}(\text{e site}^{-1}\ \text{s}^{-1})$$

$$= \frac{7.99\ (\text{mA} \cdot \text{cm}^{-2}) \times 0.19625\ (\text{cm}^{-2}) \times (14.007 + 30.974)(\text{g mol}^{-1})}{\frac{0.0911\% \times (14.007 + 30.974)}{7.5\% \times 16 + 2.83\% \times 14.007 + 88.46\% \times 12 + 1.22\% \times 30.974} \times 0.09 \times 10^{-3}(\text{g}) \times 96500\ (\text{C mol}^{-1})}$$

$$= 2.5\ \text{e site}^{-1}\ \text{s}^{-1}$$

Preparation and tests of Zn-air batteries

Schematic illustration of the Zn-air battery is shown in Figure 6a, including a polished zinc plate as an anode, N,P-HGFs-1000 catalyst (2.0 mg cm^{-2}) supported foamed nickel and waterproof and breathable membranes as air cathode, and 6 M KOH as an electrolyte. The Zn-air batteries were tested under ambient air condition (without purging O_2) at room temperature. The potential-current polarization curves for the batteries were recorded on CHI760E electrochemical workstation. The discharge performances and stability for the batteries were analyzed by the LAND CT2001A testing system.

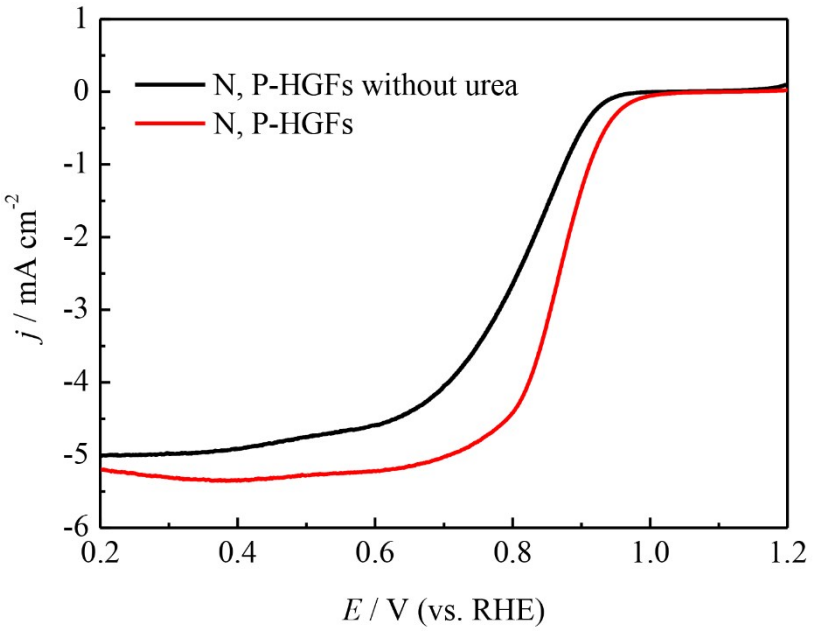

Fig. S1. RDE LSV curves for N,P-HGFs-1000 and N,P-HGFs-1000 without urea at a scan rate of 10 mV s^{-1}.

N,P-HGFs-1000 without urea shows a limited j_L and $E_{1/2}$ which are significantly lower than N,P-HGFs-1000. The reason why N,P-HGFs-1000 with urea exhibits enhanced ORR performance may be that urea not only provides more active sites as an additional source of nitrogen, but can also act as a porogen to cause an increase in specific surface area and porosity. It is speculated that the decomposition of urea at high temperatures produces gases such as CO_2 and NH_3, which in turn promotes the formation of pores.

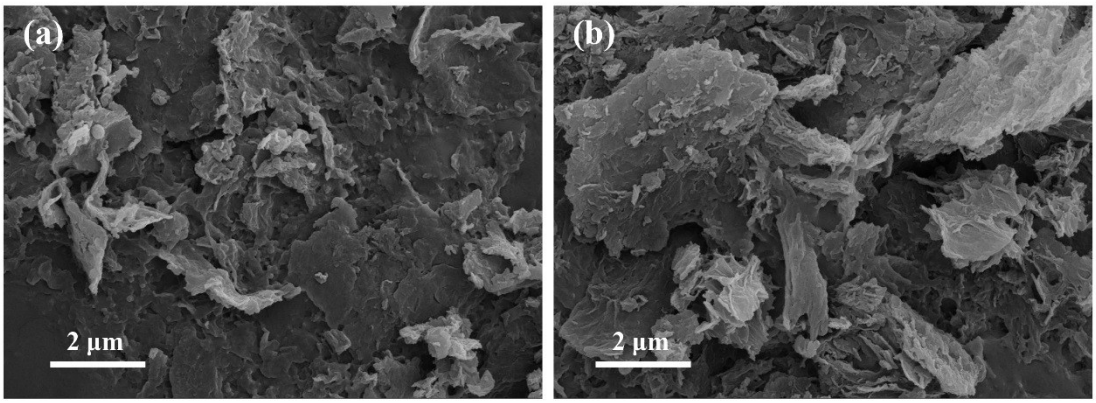

Fig. S2. SEM images of (a) N -HGFs-1000 and (b) P-HGFs-1000.

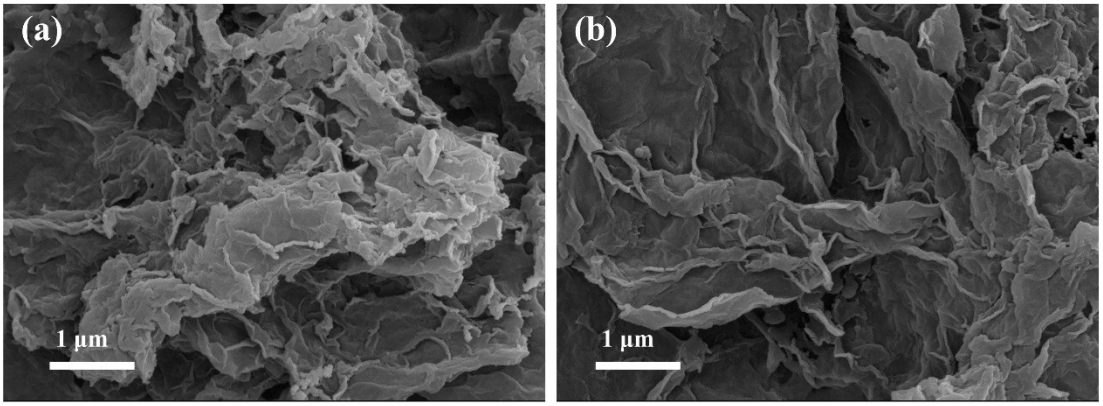

Fig. S3. SEM images of (a) N,P-HGFs-900 and (b) N,P-HGFs-1100.

A suitable pyrolysis temperature results in the best catalyst structure. Compared with N,P-HGFs-1000, N,P-HGFs-900 and N,P-HGFs-1100 all show a more regular morphology, which is not conducive to the exposure of the active site.

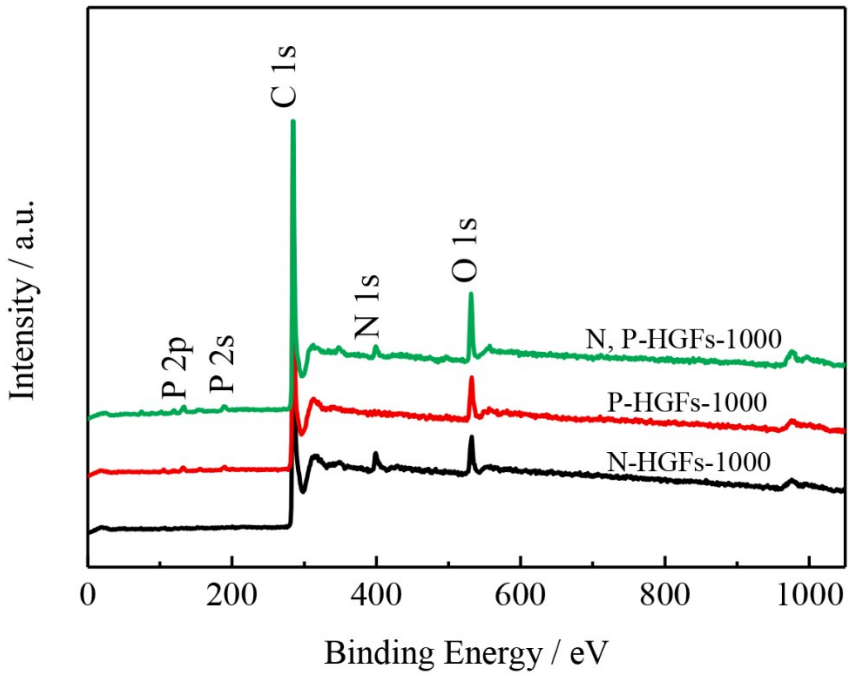

Fig. S4. XPS spectrum of P-HGFs-1000, N-HGFs-1000 and N,P-HGFs-1000.

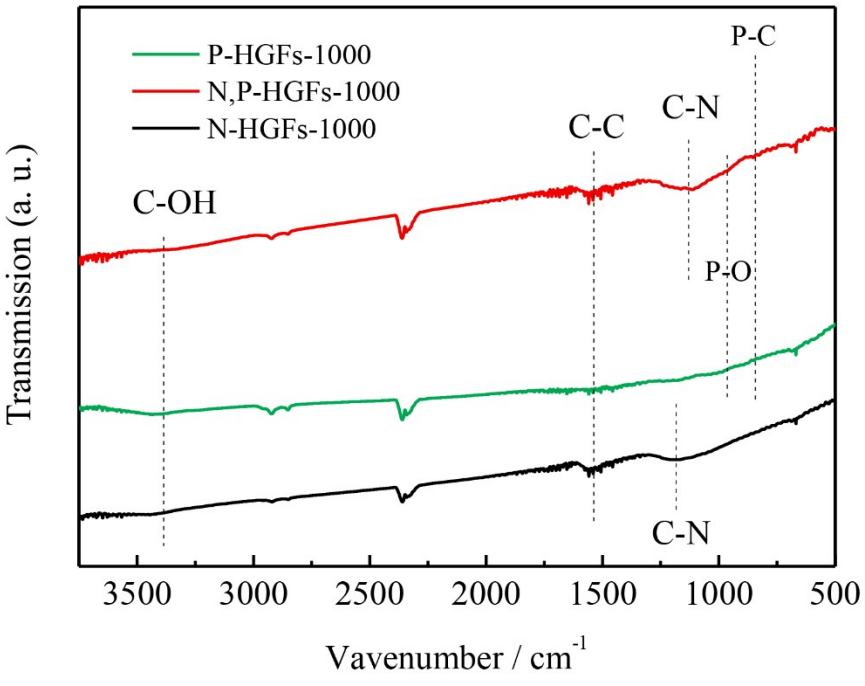

Fig. S5. Fourier transform infrared spectroscopy (FTIR) of P-HGFs-1000, N-HGFs-1000 and N,P-HGFs-1000.

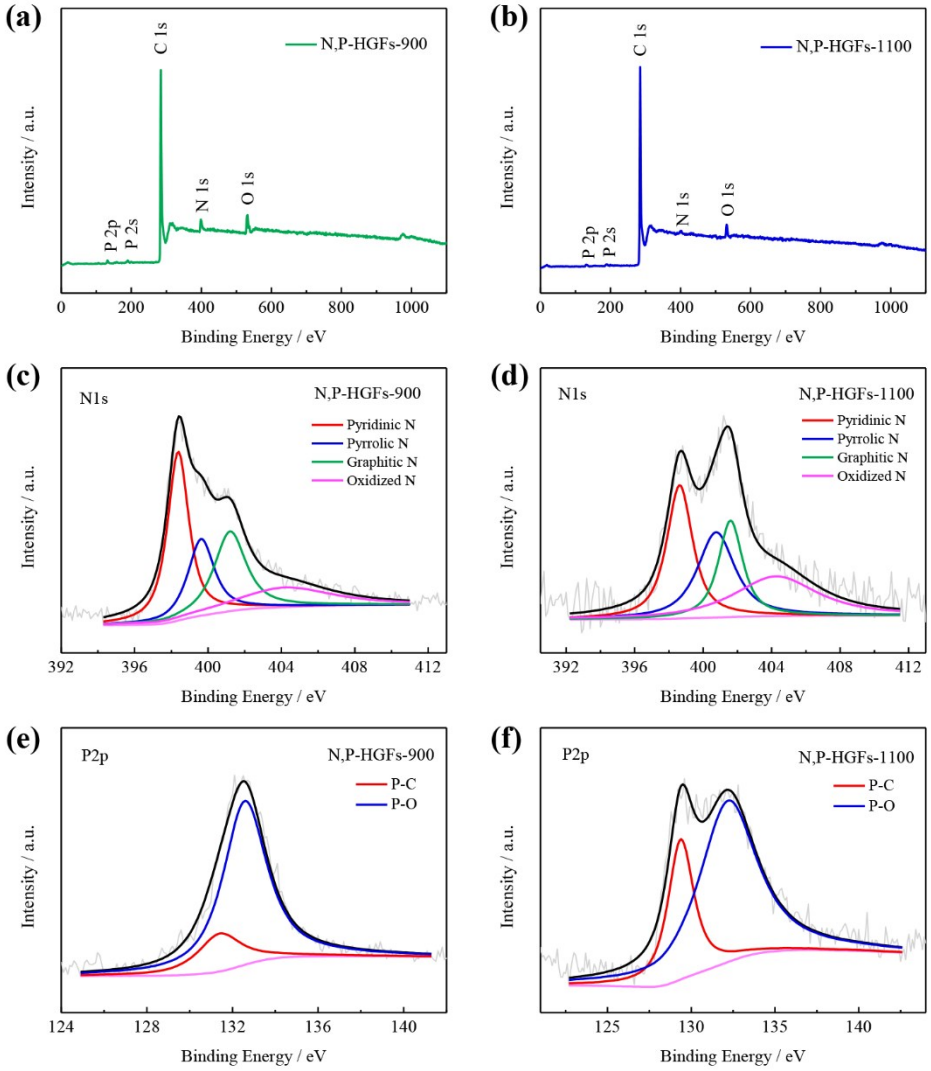

Fig. S6. (a) XPS spectrum of N,P-HGFs-900. (b) XPS spectrum of N,P-HGFs-1100. (c)High-resolution XPS spectra of N1s for N,P-HGFs-900. (d) High-resolution XPS spectra of N1s for N,P-HGFs-1100. (e) High-resolution XPS spectra of P2p for N,P-HGFs-900. (f) High-resolution XPS spectra of P2p for N,P-HGFs-1100.

The concentration of N and P can be conveniently adjusted by changing the pyrolysis temperature. The surface doping concentrations of N and P decrease as the temperature increases.

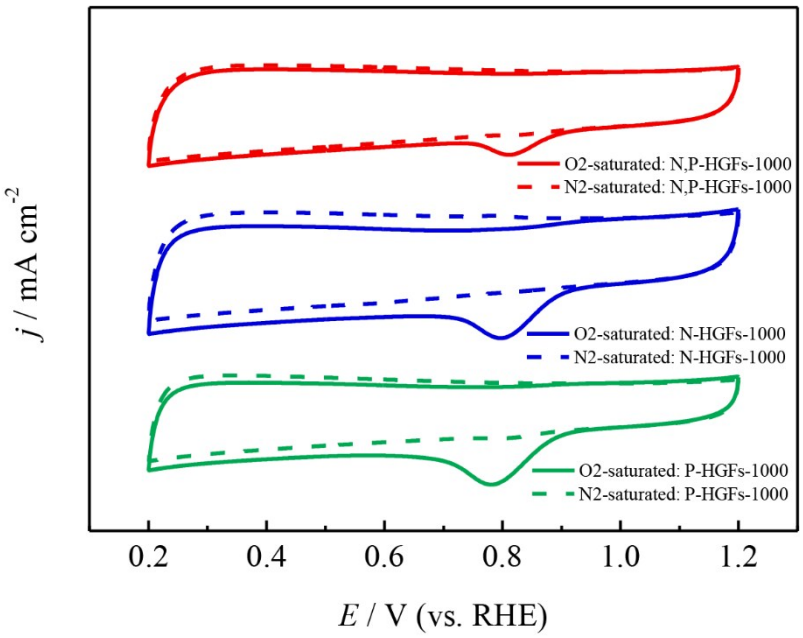

Fig. S7. CV curves of P-HGFs-1000, N-HGFs-1000 and N,P-HGFs-1000 catalysts in N_2-saturated or O_2-saturated 0.1 M KOH solution at a sweep rate of 50 mV s^{-1}

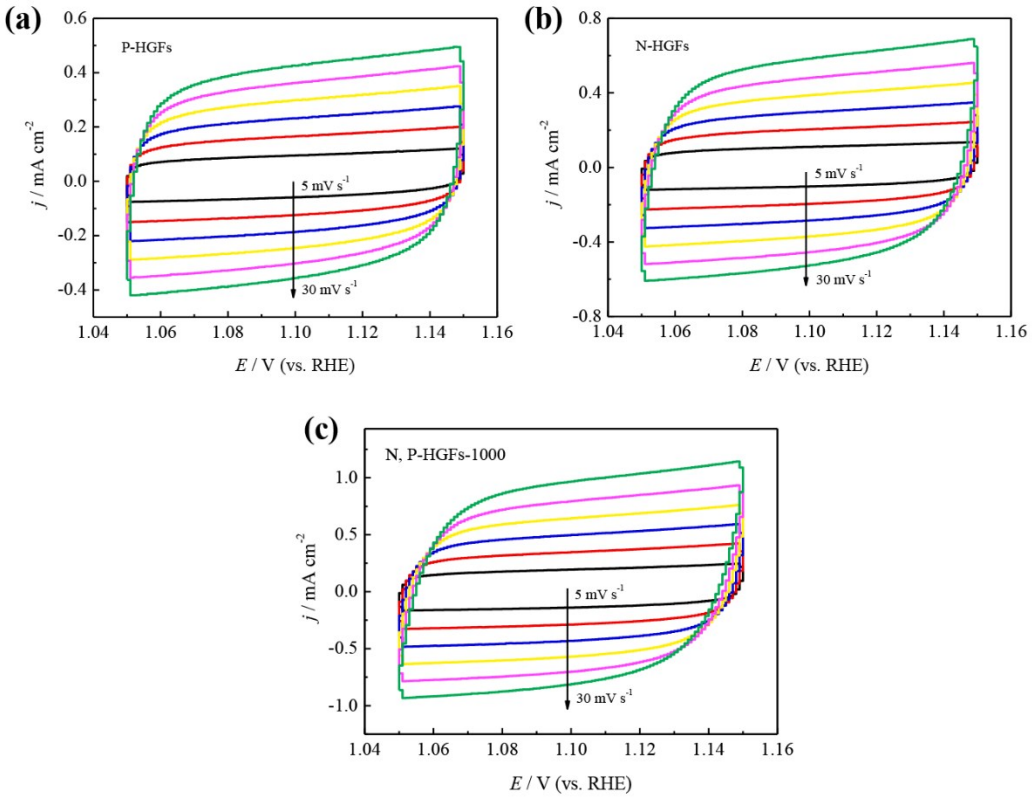

Fig. S8. CV curves of (a) P-HGFs-1000 (b) N-HGFs-1000 and (c) and N,P-HGFs-1000 at various scan rates(5, 10, 15, 20, 25,30 mV s^{-1}).

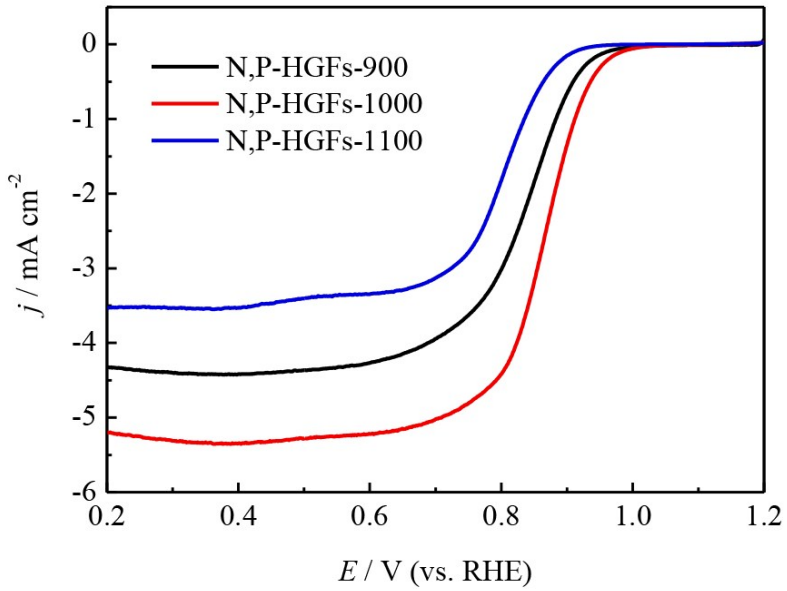

Fig. S9. RDE LSV curves for N,P-HGFs-900, N,P-HGFs-1000 and N,P-HGFs-1100 in O2-saturated at a scan rate of 10 mV s^{-1} and electrode-rotation speed of 1600 rpm.

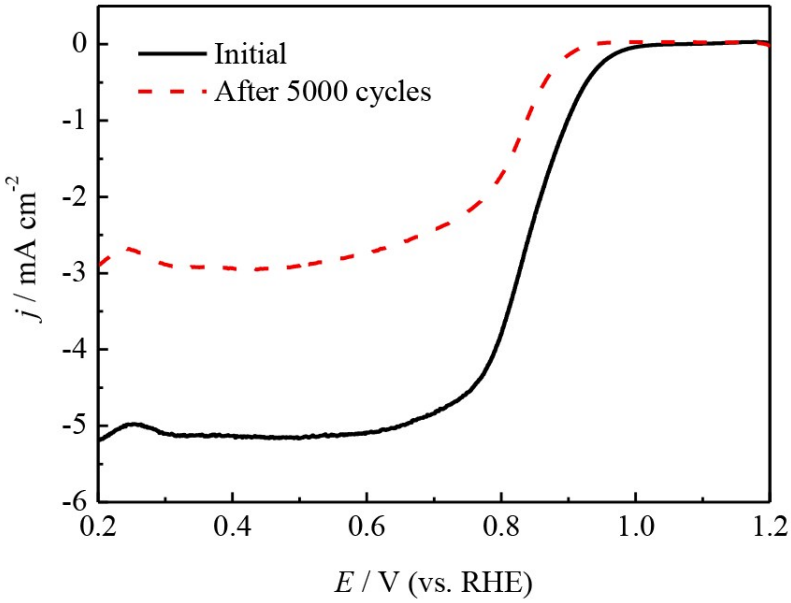

Fig. S10. ORR polarization curves before and after 5000 cycles of 20% Pt/C at 1600 rpm with a scan rate of 10 mV s^{-1}.

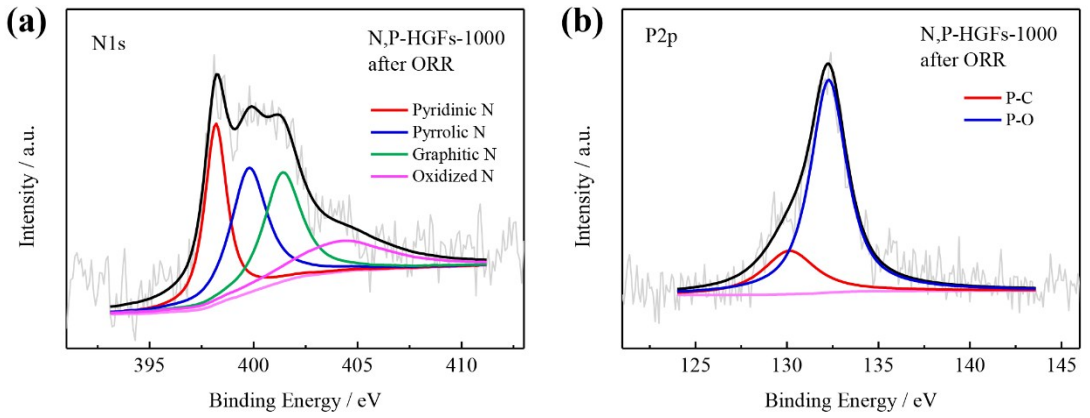

Fig. S11. (a) N1s and (b) P2p XPS spectra of the N,P-HGFs-1000 catalyst after ORR.

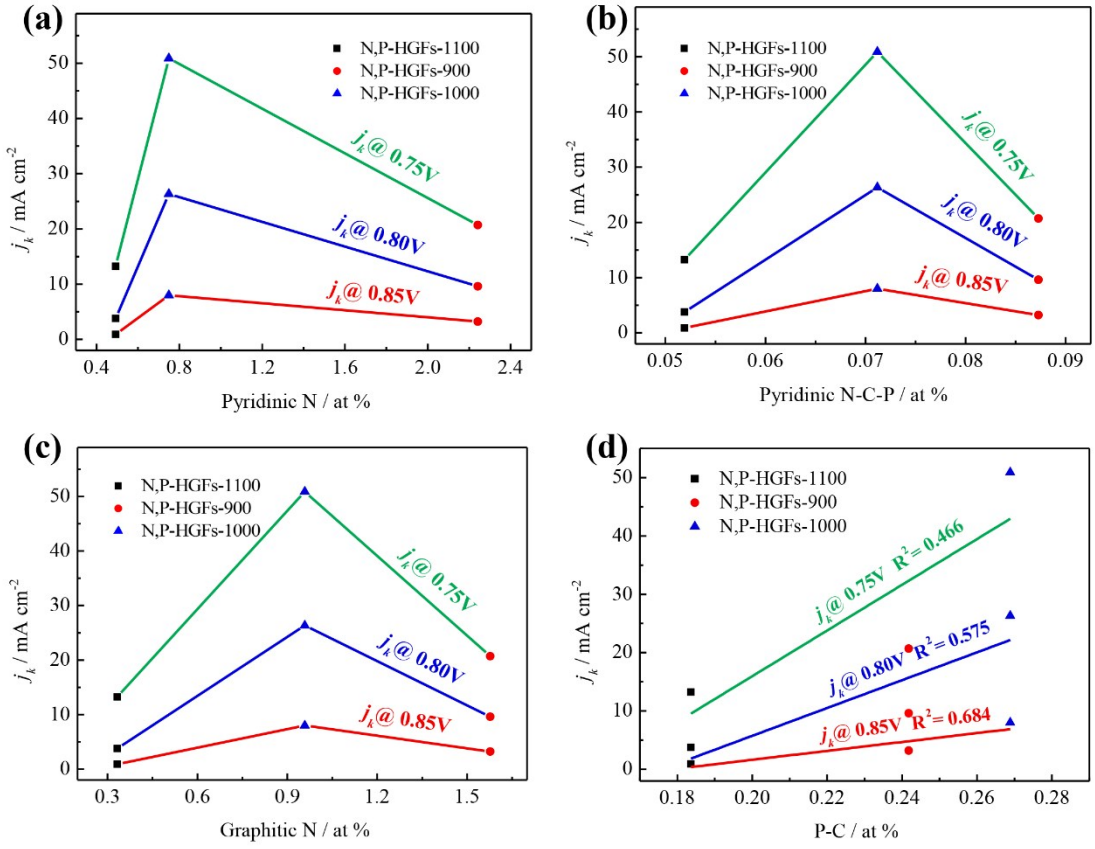

Fig. S12. Correlation between kinetic current densities of ORR at 0.85, 0.8, and 0.75 V versus RHE and the concentrations of (a) Pyridinic N species; (b) Pyridinic N-C-P species; (c) Graphitic N species; (d) P-C species.

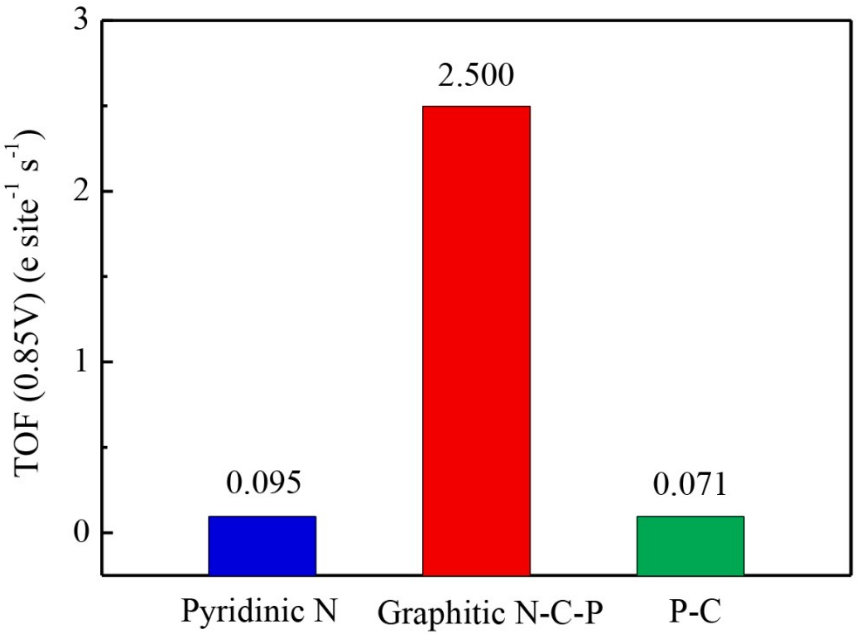

Fig. S13. Comparison of the turn-over frequency (TOF) values for Pyridinic N, P-C and Graphitic N -C-P species.

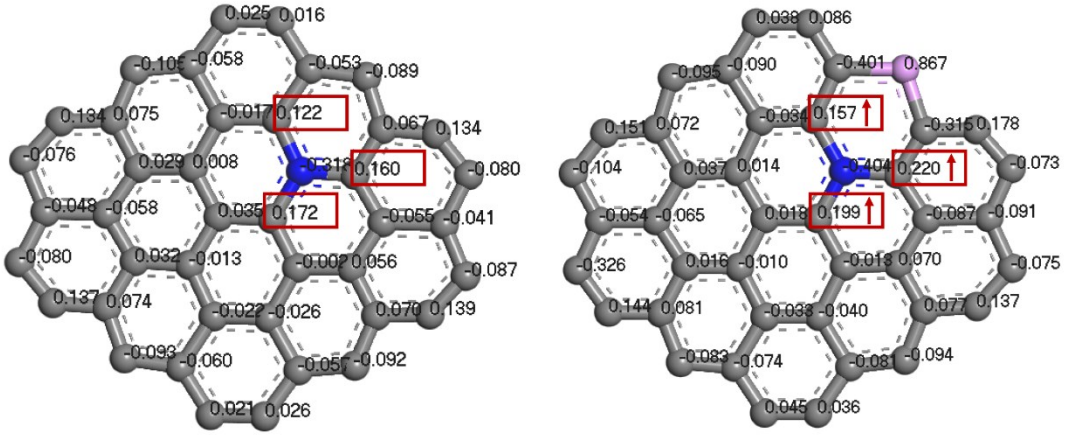

Fig. S14. Charge density of graphene network dual-doped by N and P for the graphitic N -C-P model.

Table S1. BET surfaces area, BJH adsorption main pore size and pore volume of N,P-HGFs-1000, N-HGFs-1000 and P-HGFs-1000.

Samples	BET surfaces area / m^2 g^{-1}	Pore size / nm	Pore Volume / cm^3 g^{-1}
N,P-HGFs-1000	757.7273	3.93	1.7678
N-HGFs-1000	693.0195	3.86	1.3302
P-HGFs-1000	429.8396	3.90	0.8941

Table S2. The content of C, N, O and P of t the synthesized samples obtained from XPS.

Sample	Atomic Concentration %				Mass Concentration %			
	C	N	O	P	C	N	O	P
N-HGFs-1000	90.61	4.48	4.91	-	88.51	5.1	6.39	-
P-HGFs-1000	93.55	-	5.56	0.89	90.61	-	7.17	2.22
N,P-HGFs-1000	88.46	2.83	7.5	1.22	84.34	3.14	9.52	3
N,P-HGFs-900	87.37	6.21	5.13	1.29	83.39	6.92	6.52	3.17
N,P-HGFs-1100	93.68	1.74	3.51	1.07	90.82	1.97	4.53	2.67
N,P-HGFs-1000 after ORR	88.38	1.43	9.8	0.38	84.9	1.61	12.54	0.95

Table S3. The content and type of nitrogen and phosphor of the prepared catalysts obtained from XPS.

Sample	N					P		
	Total	Graphitic N	Pyridini N	Pyrrolic N	Oxidized N	Total	P-C	P-O
N-HGFs-1000	4.48	1.78	0.94	0.90	0.87	-	-	-
P-HGFs-1000	-	-	-	-	-	0.89	0.24	0.65
N,P-HGFs-1000	2.83	0.96	0.75	0.59	0.53	1.22	0.27	0.95
N,P-HGFs-900	6.21	1.63	2.11	1.39	1.08	1.29	0.09	1.20
N,P-HGFs-1100	1.74	0.44	0.50	0.42	0.38	1.07	0.30	0.77

Table S4. Summary of the N,P co-doped carbon catalysts for ORR in alkaline medium.

Materials	$E_{1/2}$ (V) in 0.1 M KOH	References
N,P-HGFs-1000	0.865 (*vs*.RHE)	This work
PNGF(op)	0.845 (*vs*.RHE)	1
NPMC-1000	0.85 (vs.RHE)	2
N,P-GC-1000	0.85 (vs.RHE)	3
SWCNT@NPC	0.85 (vs.RHE)	4
NPCTC-850	0.83 (vs.RHE)	5
RM-COP-PA-900	0.841 (vs.RHE)	6
800-N,P-CNT	−0.162 (vs.Ag/AgCl)	7
NPHG-8	-0.34 (vs.Ag/AgCl)	8
N,P-HCS	0.81 (vs.RHE)	9
NH_3-treated NP-CT-1000	0.86 (vs.RHE)	10
N,P-CS	-0.11 (vs.Ag/AgCl)	11
N,P-NC-1000	0.83 (vs.RHE)	12
NPBC	0.85 (vs.RHE)	13
NPC1000	0.85 (vs.RHE)	14
NPC-"Li"	0.83 (vs.RHE)	15
N,P-GCNS	0.86 (vs.RHE)	16

Table S5. Summary of the performance of primary Zn-air batteries with N,P co-doped carbon catalysts.

Materials	Peak power density / mW cm^{-2}	Open-circuit Potential /V	References
N,P-HGFs-1000	103	1.452	This work
NPMC-1000	55	1.48	2
NPCTC-850	74	1.47	5
800-N,P-CNT	255	1.53	7
NPHG-8	30	1.32	8
NH_3-treated NP-CT-1000	125	1.42	10
N,P-NC-1000	146	1.48	12
NPBC	90.7	1.47	13
NP8-VACNT-GF	56	1.50	17

References

1 G.-L. Chai, K. Qiu, M. Qiao, M.-M. Titirici, C. Shang, Z. Guo, *Energy Environ. Sci.,* 2017, **10**, 1186-1195.

2 J. Zhang, Z. Zhao, Z. Xia, L. Dai, *Nat. Nanotech.*, 2015, **10**, 444-452.

3 Z. Zhou, A. Chen, X. Fan, A. Kong, Y. Shan, *Appl. Surf. Sci.*, 2019, **464**, 380-387.

4 J.-C. Li, P.-X. Hou, M. Cheng, C. Liu, H.-M. Cheng, M. Shao, *Carbon*, 2018, **139**, 156-163.

5 Y. Li, Z. Yan, Q. Wang, H. Ye, M. Li, L. Zhu, X. Cao, *Electrochim. Acta*, 2018, **282**, 224-232.

6 X. Lin, P. Peng, J. Guo, Z. Xiang, Chem. Eng. J., 2019, **358**, 427-434.

7 Z. Li, W. Zhao, C. Yin, L. Wei, W. Wu, Z. Hu, M. Wu, *ACS Appl. Mater. Inter.,* 2017, **9**, 44519-44528.

8 L. Zhou, C. Zhang, X. Cai, Y. Qian, H. Jiang, B. Li, L. Lai, Z. Shen, W. Huang, *ChemElectroChem*, 2018, **5**, 1811-1816.

9 C. Zhang, L. Hou, C. Cheng, Z. Zhuang, F. Zheng, W. Chen, *ChemElectroChem,* 2018, **5**, 1891-1898.

10 H. Li, W. Wan, X. Liu, H. Liu, S. Shen, F. Iv, J. Luo, *ChemElectroChem,* 2018, **5**, 1113-1119.

11 R. Li, H. Li, J. Long, J. He, J. Zhang, H. Zheng, X. Gou, *ChemCatChem*, 2018, **10**, 4038-4046.

12 H. Luo, W.-J. Jiang, Y. Zhang, S. Niu, T. Tang, L.-B. Huang, Y.-Y. Chen, Z. Wei, J.-S. Hu, *Carbon*, 2018, **128**, 97-105.

13 Q. Wang, Y. Li, K. Wang, J. Zhou, L. Zhu, L. Gu, J. Hu, X. Cao, *Electrochim. Acta,* 2017, **257**, 250-258.

14 X. Mao, Z. Cao, S. Chen, J. Jia, X. Li, Y. Yin, S. Yang, Int. J. *Hydrogen Energy*, 2019, **44**, 5890-5898.

15 P. Li, H. Jang, B. Yuan, Z. Wu, X. Liu, J. Cho, *Inorg. Chem. Front*., 2019, **6**, 417-422.

16 R. Li, Z. Wei, X. Gou, *ACS Catal.*, 2015, **5**, 4133-4142.

17 X. Cai, L. Lai, L. Zhou, Z. Shen, *ACS Appl. Energy Mater.*, 2019, **2**, 1505-1516.